PROCEEDINGS OF SPIE

SPIEDigitalLibrary.org/conference-proceedings-of-spie

Liquid crystal Pancharatnam-Berry optical elements

Ziyuan Zhou, Yubing Guo, Hao Yu, Miao Jiang, Taras Turiv, et al.

Ziyuan Zhou, Yubing Guo, Hao Yu, Miao Jiang, Taras Turiv, Irakli Chaganava, Oleg D. Lavrentovich, Qi-Huo Wei, "Liquid crystal Pancharatnam-Berry optical elements," Proc. SPIE 11092, Liquid Crystals XXIII, 110920D (29 August 2019); doi: 10.1117/12.2528086

SPIE.

Event: SPIE Organic Photonics + Electronics, 2019, San Diego, California, United States

Liquid Crystal Pancharatnam-Berry Optical Elements

Ziyuan Zhou[a], Yubing Guo[a], Hao Yu[a], Miao Jiang[a], Taras Turiv[a], Irakli Chaganava[b,c], Oleg D. Lavrentovich[a,d], Qi-Huo Wei[a,d]*

[a] Advanced Materials and Liquid Crystal Institute, Kent State University, Kent, OH 44240, USA

[b] Institute of Cybernetics, Georgian Technical University, 5 Sandro Euli Str., 0186 Tbilisi, Georgia

[c] Georgian State Teaching University of Physical Education and Sport, 49 Chavchavadze ave., 0179 Tbilisi, Georgia

[d] Department of Physics, Kent State University, Kent, OH 44240, USA

ABSTRACT

In this paper, we aim to show that liquid crystal films (LCs) with well-defined molecular orientations are an exceptional platform for flat optical devices based on the Pancharatnam-Berry (PB) phase. Especially, the development of plasmonic photopatterning technique in recent years has made it easy to align liquid crystal molecules in to designer orientation patterns with both high spatial resolution and high throughput and thus enables large scale manufacturing liquid crystal optical devices with low costs. Here we present liquid crystal laser beam shapers and microlenses as two examples to illustrate the design principles and the fabrication processes for liquid crystal flat optical elements. In comparison with flat optical devices made of plasmonic or dielectric metasurfaces, liquid crystal flat optical elements are advantageous due to the high optical efficiencies and low fabrication costs.

Keywords: flat optics, liquid crystal devices, Pancharatnam-Berry phase, photoalignment

1. INTRODUCTION

Metasurfaces consisting of engineered nanoscale building units are emerging as an extraordinary way to manipulate optical wave fronts[1,2]. Flat optics is highly advantageous in comparison to traditional refractive optical elements in terms of their ultra-small thickness, great flexibility in engineering wave front[3,4] and capabilities in correcting various aberrations in imaging[5]. The metasurfaces can be made by using either nanostructured plasmonic[6,7] or dielectric building units[8–10]. By varying geometric shape, orientation and size of these building units, optical amplitudes and phases can be manipulated in subwavelength scales by making use of three fundamental physical mechanisms: plasmonic or Mie resonances, waveguiding group velocities and geometric phases. Metasurfaces have been successfully engineered as flat optical elements such as lenses without aberrations and chromatic dispersions[11], holograms with high efficiency[12], and diffractive gratings[13]. Though highly successful, metasurfaces also face some limitation and challenges. The optical efficiencies of flat optical devices such as lenses based on metasurfaces are often under 80%, as a result of their discretized structures. Secondly, fabrications of metasurfaces necessitate going through a set of nanofabrication processes, making their large scale manufacturing a challenge.

The phase profiles desired for various flat optical elements can be also realized by using thin liquid crystal films based on the Pancharatnam-Berry (PB) or geometric phase. In comparison with geometric-phase-based plasmonic and dielectric metasurfaces, flat optical elements[14–17] using liquid crystal films exhibit several advantages. Firstly, the efficiency of liquid crystal flat optical devices can approach to 100%, because the continuous profiles of the geometric phases can be realized[18] and phase retardations can be precisely controlled. Secondly, due to the development of advanced techniques[19–22] to align liquid crystal molecules into designer orientations, liquid crystal films with patterned molecular orientations can be manufactured with very low cost.

In recent studies[23,24], we have shown that high quality flat optical elements can be designed and made with liquid crystal polymers by using a plasmonic photopatterning technique[19,20,25]. This paper presents a summary regarding PB phase and design principles for flat optical devices, principles and processes of the plasmonic photopatterning techniques. We use beam shapers and microlenses as two flat optical devices to illustrate the principles and advantages.

*qwei@kent.edu

Liquid Crystals XXIII, edited by Iam Choon Khoo, Proc. of SPIE Vol. 11092,
110920D · © 2019 SPIE · CCC code: 0277-786X/19/$21 · doi: 10.1117/12.2528086

2. PANCHARATNAM-BERRY PHASE AND GENERALIZED SNELL'S LAW

2.1 The Pancharatnam-Berry phase

When light passes through a birefringent material, it can acquire a phase that is related to the orientation of the principle optical axis. This phase is commonly denoted as the geometric phase, or Pancharatnam-Berry (PB) phase[26]. The PB phase can be understood with the help of Jones matrix notation. As shown in Figure 1, for a thin LC film with its slow optical axis in x-y plane and oriented with an angle θ with respect to x-axis, the Jones matrix of the film can be expressed as: $T = R(-\theta)T'R(\theta)$, where $R(\theta) = \begin{bmatrix} \cos\theta & \sin\theta \\ -\sin\theta & \cos\theta \end{bmatrix}$ is the rotation matrix and $T' = \begin{bmatrix} 1 & 0 \\ 0 & e^{-i\Gamma} \end{bmatrix}$ is the Jones matrix of the LC film when the slow optical axis is along the x-axis. The phase retardation Γ can be expressed as $\Gamma = \frac{2\pi}{\lambda}(n_e - n_o)t$, with t being the film thickness and n_e and n_o being the refractive indices for the extraordinary and ordinary beams. When $\Gamma = \pi$ or the LC film is a half wave retarder, one has $T = \begin{bmatrix} \cos 2\theta & \sin 2\theta \\ \sin 2\theta & -\cos 2\theta \end{bmatrix}$. For a circularly polarized incident light $J_{\pm} = \frac{1}{\sqrt{2}}\begin{pmatrix} 1 \\ \pm i \end{pmatrix}$, the transmitted light is:

$$J_{\pm}' = \mathrm{T} \cdot \frac{1}{\sqrt{2}}\begin{pmatrix} 1 \\ \pm i \end{pmatrix} = \frac{1}{\sqrt{2}}\begin{pmatrix} 1 \\ \mp i \end{pmatrix} e^{\pm 2i\theta}. \quad (1)$$

Here, the additional phase $\Phi = \pm 2\theta$ is the PB or geometric phase, and the exit beam has the opposite handedness. For half wave plate with uniform optical axis, the spatially uniform geometric phase exerts no influence on the propagation of light beam and thus no observable effect.

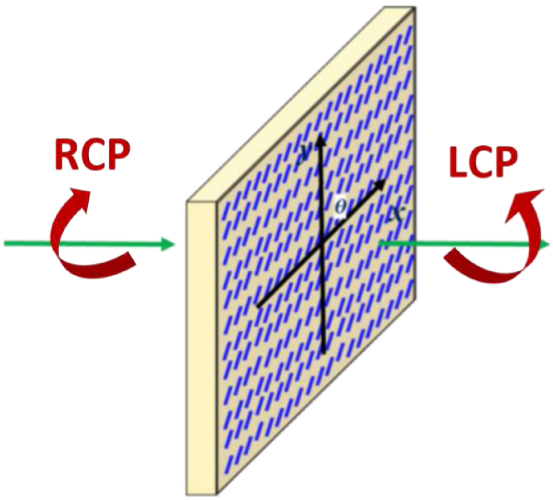

Figure 1 Pancharatnam-Berry optical devices.

2.2 The generalized Snell's law for non-uniform PB phases

When the PB phase is spatially non-uniform, the propagation direction of light beams will change. By controlling the molecular orientations, arbitrary phase profiles can be obtained with PB phase varying. Let us consider a liquid crystal film with spatially variant molecular orientations or PB phase (Fig. 2). Assuming a light beam incident on the liquid crystal film with an incident angle θ_i and a transmission angle θ_t, the Fermat's principle states that this optical path connecting two points A and B is at minimum. In another word, if the transmission point on the liquid crystal film deviates by a small distance dx, the change in optical path is zero:

$$\left[\frac{n_1}{\lambda_0}\sin(\theta_i)\,dx + (\Phi + d\Phi)\right] - \left[\frac{n_1}{\lambda_0}\sin(\theta_t)\,dx + \Phi\right] = 0 \quad (2)$$

where n_1 is the refractive index of the surrounding medium (n_1=1 for air), λ_0 is the wavelength of the incident beam in vacuum. Simple rearrangements can then yield the generalized Snell's law:

$$\sin(\theta_t) - \sin(\theta_i) = \frac{\lambda_0}{2\pi n_1}\frac{d\Phi}{dx} \tag{3}$$

Therefore, the refraction angle is only related to $\frac{d\Phi}{dx}$, the gradient of the PB phase, which is also the reason that flat optical devices (or metasurfaces) is often named gradient surfaces.

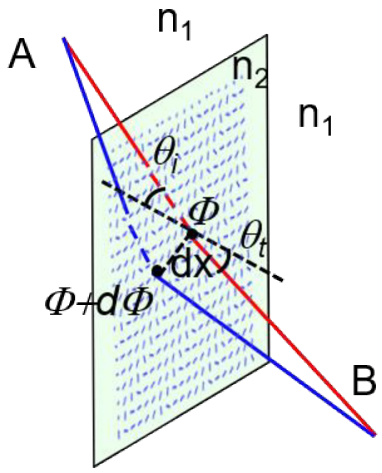

Figure 2 Derivation of the generalized Snell's law.

3. PHOTOPATTERNING OF LIQUID CRYSTAL POLYMERS

Precise control of the local orientations θ(x, y) of LC molecules is essential to achieving the desired PB phase profiles $\Phi(x, y) = 2\theta$(x, y), and thus directing light beams onto desired directions according to equation (3). Recently we developed a high resolution and high throughput photopatterning technique which enables patterning preprogrammed arbitrary 2D molecular orientations by using plasmonic metamasks (PMMS). As shown in previous works[20,25,27], these PMMs are made of rectangular nanoaperture arrays in Al films or arrays of rectangular Al parallelepipeds, and can convert broadband and non-polarized light into polarized light with predesigned patterns of polarization orientations. Basically, individual rectangular nanoapertures or parallelepipeds can be considered as polarizers, generating polarizations perpendicular to their long axes after transmission. Therefore, spatially non-uniform polarization patterns can be preprogrammed by varying the orientations of these nanoapertures or parallelepipeds. By projecting these polarization patterns onto photoalignment materials on substrates, these photo-active molecules reorient themselves to make their dipole moments perpendicular to the polarization directions. Patterned photoalignment materials can then impose their orientations into liquid crystal molecules in contact with them through van der Waals interactions. As a result, the PMMs have an extremely simple design rule, i.e. orient these rectangular apertures or parallelepipeds exactly the same as target molecular orientations. A projection photopatterning systems as shown in Fig. 3 is used for this photoalignment process.

To fabricate thin films of liquid crystal polymers with predesigned molecular orientations, we firstly spin-coated SD1, a photoalignment material with absorption band in visible range, onto cleaned glass substrate at 3000 RPM spin speed for 30 s. We then applied projection photopatterning technique with a home-built system (Fig. 3) to transfer the patterns encoded in PMMs into SD1 layer. Exposure time of this technique depends on size ratio between the patterned area in SD1 layer and that in PMM, which approximately equal to the ratio of magnifications between imaging objective and projection objective. Specifically, a 1: 1 size ratio requires exposure time of < 1 s. Subsequently, we spin-coated a toluene solution of RM257 (Wilshire technology) on top of the patterned SD1 layer and cured it with UV light in vacuum assisted with photoinitiator I651 (Ciba-Geigy Corp.) to transfer RM257 monomers into liquid crystal polymers. Thickness of the RM257 layer was monitored with Polscope and fine-tuned to reach target phase retardation for certain designed optical devices by optimized RM257 concentration and spin speed. For most optical applications, several RM257 layers from sequential spin-coating and curing process are necessary. For example, the beam shaping device and PB microlens (Section

4) require six layers of RM257 to reach the desired optical path difference of 266 nm, which is half of the working laser wavelength.

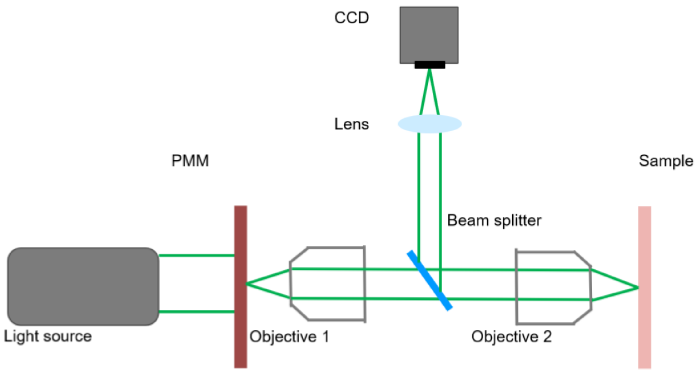

Figure 3 Projection photopatterning system.

4. EXAMPLARY FLAT OPTICAL ELEMENTS

To illustrate the concepts, we use two flat optical devices as examples: one is beam shaping devices to convert Gaussian beams into square flat-top beams, and the other is microlenses.

4.1 Beam shaping devices

The capability to shape the intensity profile of a laser beam is beneficial to various industrial applications[28]. One example is laser beams with uniform intensity distributions desired by photolithography. Here, we designed and fabricated LC beam shaping devices which converts a Gaussian laser beam into flat-top beams (Schematically shown in Figure 4a). As required by applications for convenience, the working distance f of the beam shaping devices is set to be much larger than the input beam size r_0. To find the PB phase profiles Φ(x, y) required for shaping the beams, we employed an input-output energy mapping method. Basically, we divide the target square beam area at the focal plane into $M \times M$ grids with equal spacing, and the device surface (with size of the input Gaussian beam) into $M \times M$ grids with unequal spacings to yield identical energy flux in each grid (Fig. 4a). When the light exiting from the (m_x, m_y) grid in the device plane hits the (m_x, m_y) grid in the target working focal plane and M is large enough, a laser beam with uniform intensity is generated. Since the positions of the corresponding (m_x, m_y) grids (or points when M is large) in the device plane and focal plane are known [denoted as $\boldsymbol{r}' = (x', y')$ and $\boldsymbol{r} = (x, y)$, respectively], we can use the generalized Snell's law (Eq. 3) to determine the phase gradient $\nabla\phi(x, y)$:

$$\boldsymbol{\nabla}\phi(x, y) = 2\pi(\boldsymbol{r}' - \boldsymbol{r})/\lambda_0 f \tag{4}$$

By setting the PB phase at one corner as an arbitrary constant, the desired PB phase Φ(x, y) and the molecular orientation $\theta(x, y) = \Phi(\mathrm{x}, \mathrm{y})/2$ can be determined at each mesh point.

With these orientation patterns $\theta(x, y)$, we fabricate plasmonic metamask and use it to pattern thin films of a photoalignment material (SD1) to align these photoactive molecules according these predesigned molecular orientations. Onto these photopatterned alignment films, we spin-casted reactive mesogens (RM257, Wilshire technology) mixed with photo-initiator I651 (CIBA-GEIGY Corp.) and photopolymerized them at room temperature. The film thicknesses were controlled to yield half wave phase retardation at wavelength λ_0 = 532 nm. Figure 4b and 4c present polarizing optical microscopic images of the fabricated plasmonic metamask and a LC beam shaping device, respectively.

We build an optical system to characterize the LC beam shaping device as shown in Figure 4d. A Gaussian beam with wavelength $\boldsymbol{\lambda_0}$=532nm from a solid-state laser is transformed into circular polarized light by a combination of a polarizer and a quarter waveplate. Then two lenses are used to reduce the beam size from $\boldsymbol{r_0}$=742 μm to $\boldsymbol{r_0}$ =150 μm, which is the

size of the LC beam shaping device. A pinhole with 100 μm diameter is placed between these two lenses to clean up the beam. The LC beam shaping device is placed at the waist of the laser beam where the wavefront is a flat plane. A microscope system composed of an objective, a tube lens and a CCD camera are used to image the laser beam at the target focal plane. Figure 4e shows the image taken by the CCD camera, showing well-defined flat-top beam. Details of the intensity profile is presented in the 3D view (Figure 4f).

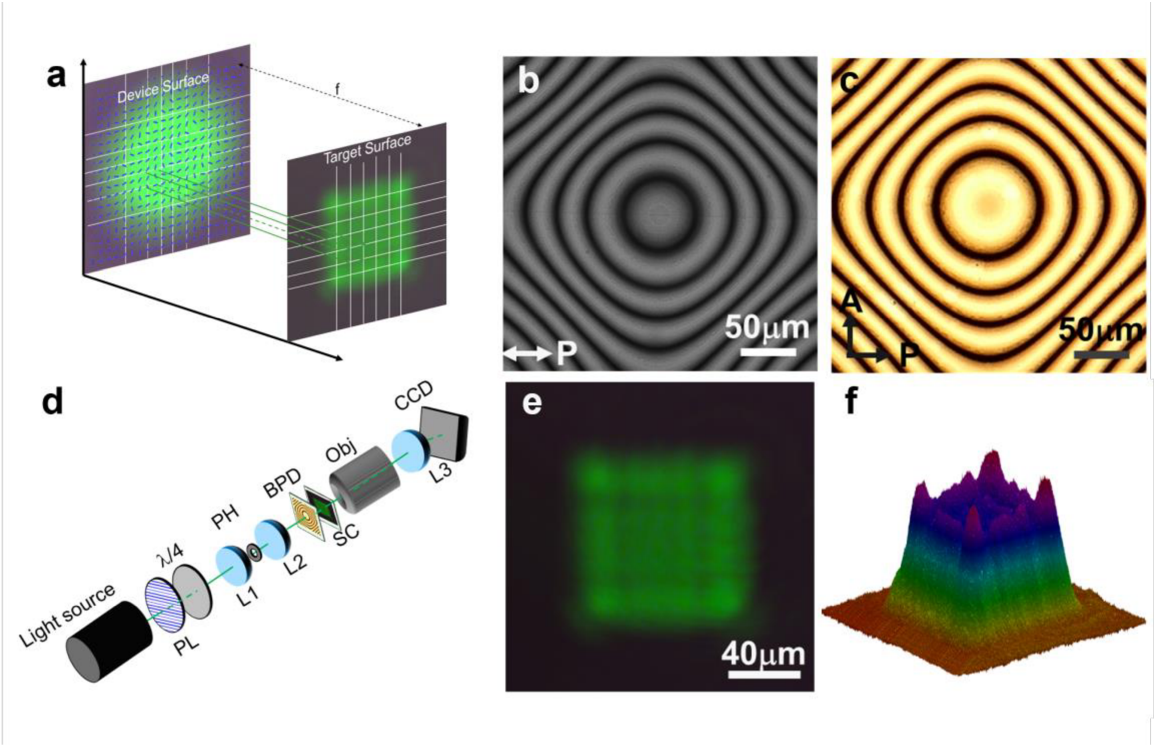

Figure 4 Liquid crystal beam shaping device. (a) Intensity mapping method for calculating the PB phase profiles. (b) Microscopic image of the PMM. (c) Polarizing microscopic image of the LC beam shaper fabricated by using the PMM in (b). (d) Schematic of the optical setup for characterizing the LC beam shaping devices. PL: polarizer; λ/4: quarter wave plate; L1: lens with f = 130 mm; PH: pinhole; L2: lens with f = 50 mm; BPD: beam shaping device; SC: screen; L3: lens with f = 100 mm; OB: objective. (e) Measured intensity distribution of the beam shaper in (c) at the working plane for a 532 nm laser. (f) 3D perspective view of the laser intensity profile in (e).

4.2 Microlenses

Microlenses with submillimeter diameters are essential optical components in an extensive variety of miniaturized system applications such as wave front sensing, beam homogenization and virtual/augmented reality[15,29–31]. In our previous publications [18,24], we have demonstrated that microlenses can be well realized based on the Pancharatnam-Berry phase with the help of the plasmonic photopatterning technique. Similar to the beam shaping device, the propagation direction of transmitted light is dictated by local gradient of the geometric phase, the phase profile or molecular orientation pattern required for a microlens can be easily obtained by combining the geometric condition $\sin(\theta_t) = r/\sqrt{r^2 + f^2}$ (Fig. 5a) with Eq. 3:

$$\Phi(r) = 2\theta(r) = \frac{2\pi}{\lambda_0}\left(\sqrt{f^2 + r^2} - f\right) \quad (5)$$

where Φ, θ, f, r, λ_0 are the PB phase, local molecular orientations, focal length, distance to the microlens center and the working wavelength in the surrounding media, respectively.

With Eq. 5, we designed microlenses with a set of f-numbers and focal lengths. The fabrication process is similar to the process for fabricating beam shaping devices in 4.1. Fig. 5b and 5c present exemplary optical microscopic images of a PMM and a LC PB microlens fabricated with the PMM.

The performances of the PB microlenses were characterized by using an optical setup schematically shown in Fig. 5d. The focused laser spot is imaged onto a CCD camera with an objective (Obj) and a tube lens (L3). For coherent light, the electrical field distribution imaged at the CCD camera is the convolution between the electrical field amplitude point spread function $g(\mathbf{r})$ of the objective and the electrical field distribution f($\mathbf{r}$) of the PB lens, and thus the measured intensity distribution can be expressed as:

$$I(\mathrm{x},\mathrm{y}) = I_0\left[\iint_{-\infty}^{\infty} \mathrm{f}(\mathbf{r}')g(\mathbf{r}-\mathbf{r}')d\mathbf{r}'\right]^2 \tag{6}$$

As the microscope objective used is diffraction-limited, its amplitude point spread function is an Airy pattern due to diffraction by a circular aperture, or $g(\boldsymbol{r}) = J_1(kr)/kr$, where J_1 is the first order Bessel function; $k = \pi \cdot N_A/\lambda_0$ with $\mathrm{N_A}$ being the numerical aperture of the objective. For the microlens of a square shape with width l, the far-field amplitude at the focal spot results from Fraunhofer diffraction, and thus $f(\boldsymbol{r}) = \sin\alpha x * \sin\alpha y/(\alpha x * \alpha y)$, where $\alpha = \pi\, l/f\lambda_0$. The focal spot of the PB lens is shown in Fig. 5e, and its intensity profile along the horizontal line through the spot center is plotted in Fig. 5f with blue empty shapes while the calculated convolution are plotted with red line. It can be seen that the experimental data can be well fitting using Eq. 6 with experimental parameters (l, f, λ_0, N_A), implying that the size of the focal spot is limited by diffraction.

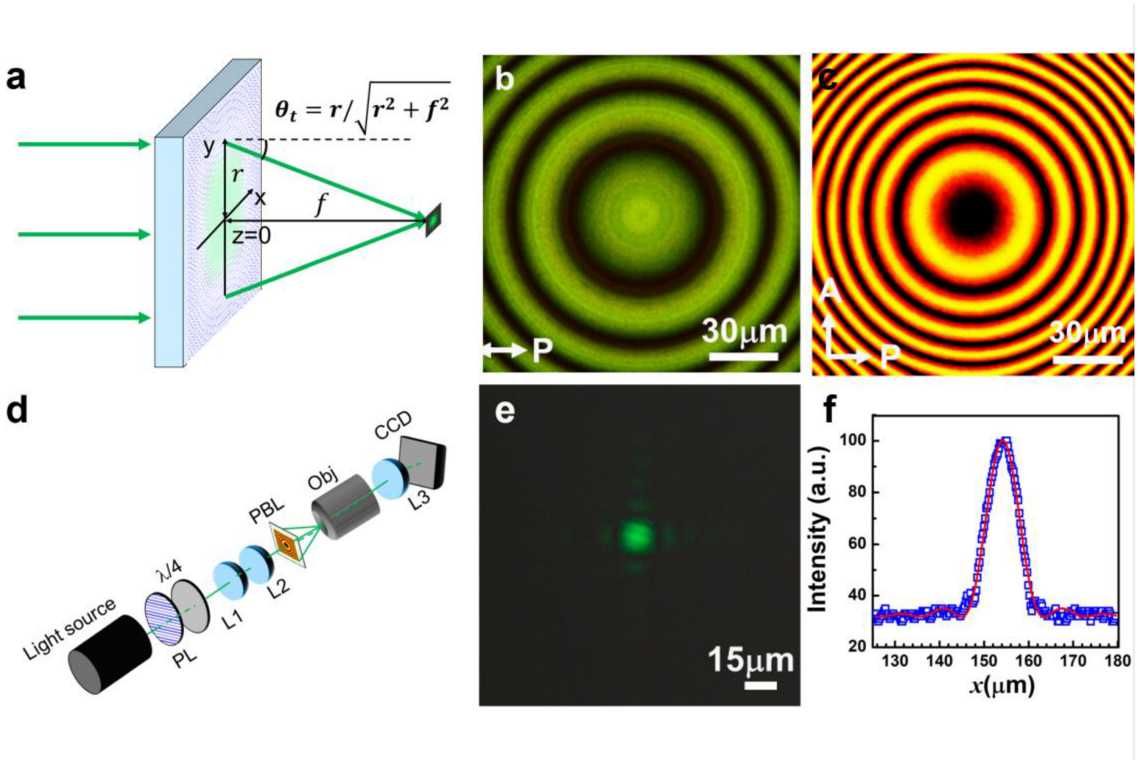

Figure 5 (a) Geometric condition of a typical lens. (b) Microscopic image of a PMM for a square microlens with 150 μm size and 2250 μm focal length. (c) Polarizing microscopic image of ta microlens fabricated with liquid crystal polymer with the PMM in (b). (d) Schematic optical setup for characterizing the point spread function (PSF) of the PB microlenses. (e) PSF of the microlens in (c) at the focal plane with illumination of a 532 nm solid state laser. (f) Measured intensity profile across the focal spot in (e) (blue empty shapes) and the calculated convolution fitting with Eq. 6 (red line).

5. CONCLUSIONS

To conclude, we have shown that flat liquid crystal optical devices such as beam shapers and microlenses can be designed and fabricated based on engineering the profiles of Pancharatnam-Berry phases (or geometric phases). By using the Generalized Snell's law, the phase profiles and thus molecular orientations for these optical devices can be pre-designed with high accuracy. With the plasmonic photopatterning technique, these liquid crystal flat optical devices can be made with high resolution and high throughput and are viable for practical deployments for practical use.

ACKNOWLEDGMENTS

This work is supported by the National Science Foundation (NSF) through CMMI-1663394 and CMMI-1436565.

REFERENCES

[1] Chen, H. T., Taylor, A. J. and Yu, N., "A review of metasurfaces: Physics and applications," Reports Prog. Phys. **79**(7) (2016).

[2] Ding, F., Pors, A. and Bozhevolnyi, S. I., "Gradient metasurfaces: A review of fundamentals and applications," Reports Prog. Phys. **81**(2) (2018).

[3] Yu, N. and Capasso, F., "Flat optics with designer metasurfaces," Nat. Mater. **13**(2), 139–150 (2014).

[4] Martini, E., Mencagli, M., González-Ovejero, D. and Maci, S., "Flat optics for surface waves," IEEE Trans. Antennas Propag. **64**(1), 155–166 (2016).

[5] Aieta, F., Genevet, P., Kats, M. A., Yu, N., Blanchard, R., Gaburro, Z. and Capasso, F., "Aberration-free ultrathin flat lenses and axicons at telecom wavelengths based on plasmonic metasurfaces," Nano Lett. (2012).

[6] Tan, S. J., Zhang, L., Zhu, D., Goh, X. M., Wang, Y. M., Kumar, K., Qiu, C. W. and Yang, J. K. W., "Plasmonic color palettes for photorealistic printing with aluminum nanostructures," Nano Lett. **14**(7), 4023–4029 (2014).

[7] Ni, X., Kildishev, A. V. and Shalaev, V. M., "Metasurface holograms for visible light," Nat. Commun. **4**, 1–6 (2013).

[8] Lin, D., Fan, P., Hasman, E. and Brongersma, M. L., "Dielectric gradient metasurface optical elements," Science. **345**(6194), 298–302 (2014).

[9] Kuznetsov, A. I., Miroshnichenko, A. E., Brongersma, M. L., Kivshar, Y. S. and Luk'yanchuk, B., "Optically resonant dielectric nanostructures," Science. **354**(6314) (2016).

[10] Arbabi, A., Horie, Y., Bagheri, M. and Faraon, A., "Dielectric metasurfaces for complete control of phase and polarization with subwavelength spatial resolution and high transmission," Nat. Nanotechnol. **10**(11), 937–943 (2015).

[11] Aieta, F., Kats, M. A., Genevet, P. and Capasso, F., "Multiwavelength achromatic metasurfaces by dispersive phase compensation," Science. **347**(6228), 1342–1345 (2015).

[12] Huang, L., Chen, X., Mühlenbernd, H., Zhang, H., Chen, S., Bai, B., Tan, Q., Jin, G., Cheah, K. W., Qiu, C. W., Li, J., Zentgraf, T. and Zhang, S., "Three-dimensional optical holography using a plasmonic metasurface," Nat. Commun. **4**(May), 1–8 (2013).

[13] Bomzon, Z., Biener, G., Kleiner, V. and Hasman, E., "Radially and azimuthally polarized beams generated by space-variant dielectric subwavelength gratings," Opt. Lett. **27**(5), 285 (2002).

[14] Kobashi, J., Yoshida, H. and Ozaki, M., "Planar optics with patterned chiral liquid crystals," Nat. Photonics **10**(6), 389–392 (2016).

[15] Zhan, T., Lee, Y.-H. and Wu, S.-T., "High-resolution additive light field near-eye display by switchable Pancharatnam–Berry phase lenses: errata," Opt. Express **26**(22), 28505 (2018).

[16] He, Z., Lee, Y.-H., Chen, R., Chanda, D. and Wu, S.-T., "Switchable Pancharatnam–Berry microlens array with nano-imprinted liquid crystal alignment," Opt. Lett. **43**(20), 5062 (2018).

[17] Gao, K., Cheng, H.-H., Bhowmik, A. K. and Bos, P. J., "Thin-film Pancharatnam lens with low f-number and high quality," Opt. Express **23**(20), 26086 (2015).

[18] Yu, H., Zhou, Z., Qi, Y., Zhang, X. and Wei, Q.-H., "Pancharatnam–Berry optical lenses," J. Opt. Soc. Am. B **36**(5), D107 (2019).

[19] Yu, H., Jiang, M., Guo, Y., Turiv, T., Lu, W., Ray, V., Lavrentovich, O. D. and Wei, Q. H., "Plasmonic Metasurfaces with High UV–Vis Transmittance for Photopatterning of Designer Molecular Orientations," Adv. Opt. Mater. **7**(11), 1–8 (2019).
[20] Guo, Y., Jiang, M., Peng, C., Sun, K., Yaroshchuk, O., Lavrentovich, O. and Wei, Q. H., "High-Resolution and High-Throughput Plasmonic Photopatterning of Complex Molecular Orientations in Liquid Crystals," Adv. Mater. **28**(12), 2353–2358 (2016).
[21] White, T. J., Wie, J. J., McConney, M. E., Ware, T. H. and Tondiglia, V. P., "Voxelated liquid crystal elastomers," Science (80-.). **347**(6225), 982–984 (2015).
[22] Xia, Y., Cedillo-Servin, G., Kamien, R. D. and Yang, S., "Guided Folding of Nematic Liquid Crystal Elastomer Sheets into 3D via Patterned 1D Microchannels," Adv. Mater. **28**(43), 9637–9643 (2016).
[23] Jiang, M., Yu, H., Feng, X., Guo, Y., Chaganava, I., Turiv, T., Lavrentovich, O. D. and Wei, Q. H., "Liquid Crystal Pancharatnam–Berry Micro-Optical Elements for Laser Beam Shaping," Adv. Opt. Mater. **6**(23), 1–7 (2018).
[24] Jiang, M., Guo, Y., Yu, H., Zhou, Z., Turiv, T., Lavrentovich, O. D. and Wei, Q. H., "Low f-Number Diffraction-Limited Pancharatnam–Berry Microlenses Enabled by Plasmonic Photopatterning of Liquid Crystal Polymers," Adv. Mater. **31**(18), 1–7 (2019).
[25] Guo, Y., Jiang, M., Peng, C., Sun, K., Yaroshchuk, O., Lavrentovich, O. and Wei, Q.-H., "Designs of Plasmonic Metamasks for Photopatterning Molecular Orientations in Liquid Crystals," Crystals **7**(1), 8 (2016).
[26] Berry, M. V., "The Adiabatic Phase and Pancharatnam's Phase for Polarized Light," J. Mod. Opt. **34**(11), 1401–1407 (1987).
[27] Yu, H., Jiang, M., Guo, Y., Turiv, T., Lu, W., Ray, V. and Lavrentovich, O. D., "Plasmonic Metasurfaces with High UV – Vis Transmittance for Photopatterning of Designer Molecular Orientations," Adv. Opt. Mater. **7**, 1900117 (2019).
[28] Dickey, F. M., Holswade, S. C. and Shealy, D. L., eds., [Laser Beam Shaping Applications], CRC Press (2018).
[29] Artzner, G., "Microlens arrays for Shack-Hartmann wavefront sensors" (1992).
[30] Wippermann, F., Zeitner, U.-D., Dannberg, P., Bräuer, A. and Sinzinger, S., "Beam homogenizers based on chirped microlens arrays," Opt. Express **15**(10), 6218 (2007).
[31] Lee, Y.-H., Tan, G., Zhan, T., Weng, Y., Liu, G., Gou, F., Peng, F., Tabiryan, N. V., Gauza, S. and Wu, S.-T., "Recent progress in Pancharatnam–Berry phase optical elements and the applications for virtual/augmented realities," Opt. Data Process. Storage **3**(1), 79–88 (2017).